Natural Resources Canada | Ressources naturelles Canada

GEOMATICS CANADA
OPEN FILE 44

A catalogue of potential natural oil seeps in the marine environment of Hudson Bay–Hudson Strait and Foxe Channel from 2015–2017 RADARSAT-2 imagery analysis

M. Beauchemin, S. Tolszczuk-Leclerc, V. Decker, P. Muise, S.K. Khurshid, and D. Hennessy

2018

Canada

GEOMATICS CANADA

OPEN FILE 44

A catalogue of potential natural oil seeps in the marine environment of Hudson Bay–Hudson Strait and Foxe Channel from 2015–2017 RADARSAT-2 imagery analysis

M. Beauchemin[1], S. Tolszczuk-Leclerc[1], V. Decker[1], P. Muise[1], S.K. Khurshid[2], and D. Hennessy[1]

[1] Canada Centre for Mapping and Earth Observation, Canada Centre for Remote Sensing, 560 Rochester Street, Ottawa, Ontario K1A 0E4
[2] Environment and Climate Change Canada, 373 Sussex Drive, Ottawa, Ontario K1A 0H3

2018

Permanent link: https://doi.org/10.4095/308463

This publication is available for free download through GEOSCAN (http://geoscan.nrcan.gc.ca/).

Recommended citation

Beauchemin, M., Tolszczuk-Leclerc, S., Decker, V., Muise, P., Khurshid, S.K., and Hennessy, D., 2018. A catalogue of potential natural oil seeps locations in the marine environment of Hudson Bay–Hudson Strait and Foxe Channel from 2015–2017 RADARSAT-2 imagery analysis; Geomatics Canada, Open File 44, 1 .zip file. https://doi.org/10.4095/308463

Publications in this series have not been edited; they are released as submitted by the author.

ABSTRACT

We report results from the analysis of Radarsat-2 images for the detection of suspected oil slicks in the marine environment of Hudson Bay/Strait and Foxe Channel. 1278 images were acquired during the falls of 2015, 2016 and 2017. The potential slick candidates were identified using two methods: visual interpretation and semi-automated interpretation. The visual method is similar to the ones described in Decker et al. (2013a, b). The semi-automated approach is based on a suite of algorithms designed to detect and characterize dark areas. Both methods make use of wind speed and chlorophyll-*a* data. A total number of 33 oil slicks candidates are reported with their locations and corresponding images. The ultimate goal of the multi-temporal aspect of the project was to look for persistence over time of seep candidates concentrated over a same region in order to assist in finding regions with a greater likelihood of oil seep origin. The current survey does not convincingly support the oil seep origin of any detected dark spot but may help future works focus on the few areas that show more dense occurrences of slick candidates.

RÉSUMÉ

Nous présentons les résultats de l'analyse d'images Radarsat-2 pour la détection de nappes de pétrole présumées dans l'environnement marin de la baie d'Hudson / détroit et du chenal de Foxe. 1278 images ont été acquises lors des automnes de 2015, 2016 et 2017. Les candidats potentiels ont été identifiés selon deux méthodes: l'interprétation visuelle et l'interprétation semi-automatique. La méthode visuelle est similaire à celles décrites dans Decker et al. (2013a, b). L'approche semi-automatisée est basée sur une suite d'algorithmes conçus pour détecter et caractériser les zones sombres. Les deux méthodes utilisent la vitesse du vent et les données de chlorophylle-α. Un total de 33 candidats possible de nappes de pétrole sont reportés avec leurs emplacements et les images correspondantes. Le but ultime de la composante multi-temporel du projet était de rechercher la persistance temporelle des candidats concentrés dans une même région afin d'aider à trouver des régions avec une plus grande probabilité d'origine de suintement pétrolier. L'étude actuelle ne soutient pas de manière convaincante l'origine de suintement d'huile d'aucune tache noire détectée, mais pourrait aider les travaux futurs à se concentrer sur les quelques zones qui présentent des occurrences plus denses.

Table of Content

List of Tables

List of Figures

1. INTRODUCTION

This report builds on work initiated by Decker et al. (2013a, b) under the first phase of the Geoscience for Energy and Minerals (GEM-1) program. The latter analyzed Radarsat-2 satellite images to identify suspected oil slicks from dark areas detected on the water surface for monitoring and assessing the hydrocarbon potential of Hudson Bay and Foxe Basin. The rationale for this approach is that, under favorable wind conditions, water surfaces covered by oil films would appear as dark areas on C-band SAR images with incidence angles between 23 and 50 degrees, such as with Radarsat-2 images. Decker et al. (2013a, b) report the location of 40 suspect dark targets derived from the visual interpretation of 360 images acquired between 2010 and 2012. The present work further investigates the oil seep occurrence in the same regions with the analysis of 1278 Radarsat-2 images acquired during the falls of 2015, 2016 and 2017 (beginning of August to the end of October). The ultimate goal of the multi-temporal aspect of the project is to identify possible persistence over time of dark spots in a restricted area to strengthen their hydrocarbon origin. The potential slick candidates were identified through two methods: visual interpretation and semi-automated interpretation. The visual method is primarily based on the work described in Decker et al. (2013a, b). The semi-automated approach was developed to automatically detect and characterize dark areas image properties. Both methods make use of wind speed and chlorophyll-*a* data to help exclude false positive from the analysis. The greatest challenge in oil slick detection using single polarization SAR imagery is the presence of look-alikes (Alpers et al. 2017). Look-alikes are dark areas on open waters in SAR images that have a similar appearance to oil slicks but have non-petroleum origins. Natural phenomena that lead to look-alikes include (Topouzelis 2008): low wind zones, organic film, atmospheric fronts, rain cells, grease ice, internal waves, upwelling and down-welling zones, areas sheltered by land, and eddies. Ancillary data such as local wind speeds and chlorophyll-*a* data becomes thus of great help to screen out probable look-alikes (Alpers et al. 2017).

We report a total number of 33 oil slicks candidates with their locations and corresponding images (the geospatial data is also available as a zipped geospatial ESRI™ shape file). We also discuss the result of a spatio-temporal analysis conducted on these candidates. In the following report, the terms ‘dark target’ and ‘dark spot’ are used interchangeably and refers to a dark area in the image. Oil slick or seep candidates refers to dark spots that have image properties of verified oil slicks in the scientific literature, mainly the level of darkness, texture, context and shape.

2. Radarsat-2 images and coverage

All images were acquired in VV polarization with a spatial resolution 12.5m (wide mode, SGF product). Each image covers an area of 150 ×150 km^2. There were 434 images acquired in 2015, 440 images in 2016, and 404 images in 2017 for a total number of 1278 images. All images were obtained during expected ice free conditions, i.e. August, September and October of each year. A sample of radar image footprints of the area surveyed are shown in Figure 1, only the month of September of each year is displayed to improve clarity. The month of September also corresponds to peak coverage each year, September being at the height of the ice free season. The number of different images acquired over the exact same location varies within the covered

area and is, on average, 22 images over the three years with a minimum of 7 and a maximum of 43 images.

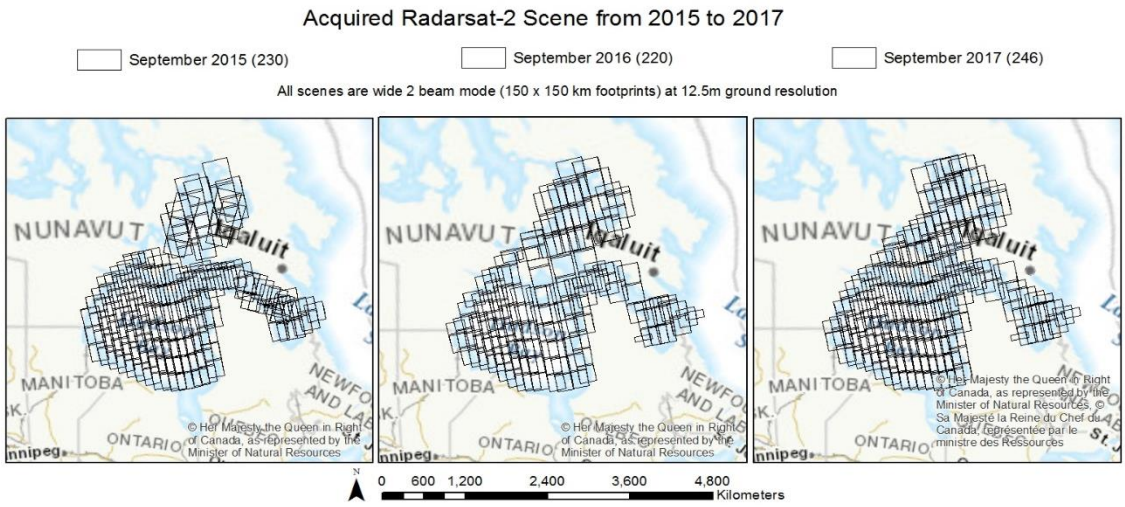

Figure 1. Radarsat-2 area coverage (Radarsat-2 image footprints).

3. METHODOLOGY

Two different approaches to dark spot detection were used in this study. One technique is based on visual interpretation of the entire image set. The second method relies on a semi-automated method for dark spot detection on the entire image set. To minimize the amount of look-alikes, local wind speeds and chlorophyll-*a* data were included in the analysis for both approaches. Notice that, although chlorophyll-*a* and wind speeds data have uncertainties, they were used as they were accurate. Consequently, there is a probability that some potential oil slicks be missed in the process when chlorophyll-*a* or low/high wind speeds are falsely detected.

Localized persistence of dark spots over time constitutes another clue to support a petroleum origin and this is also considered in the present work. Each method is described next.

3.1 Visual interpretation

The visual interpretation approach is similar to the ones described in Decker et al. (2013a,b). Each images was geocoded, filtered with a 3 × 3 median filter, then enhanced with a minimum-maximum linear contrast stretch. Then, images were merged together into a single mosaic for each orbital pass. This process was mainly developed in python/ArcGIS during phase one of the Geomapping for Energy and Minerals (GEM-1) program of the Canadian Geological

Commission. All image mosaics were subsequently visually inspected. Each Radarsat-2 mosaic was displayed on two large monitors, a small portion at a time. Further visual enhancement techniques were applied if necessary.

The study area has no known oil seeps to act as a ground truth; therefore, the interpreter used examples of known oil seeps and look-alikes taken from scientific literature as a comparison basis. The locations of potential slicks were marked using rectangular boxes encapsulating isolated slicks or tight group of slicks and then registered into a GIS database with an associated confidence level. The interpreter used the following subjective ranking system to assign a confidence level to each dark spot:

1. Best candidate: *i*) a dark feature located either near a known an active seep,

   ii) a dark feature with clearly defined boundaries and observed far from weak features resembling biological processes or wind effects.

2. Unknown origin:

   i) a dark spot that could be explained by the presence of a seep or other phenomena,

   ii) a dark feature with high contrast boundaries observed close from weak features resembling ocean surface or biological processes.

3. Weak candidate:

   i) Unlikely to be of hydrocarbon origin: a dark feature that is likely the result of phenomena other than a hydrocarbon seep. It is included in the database until more information can rule it out with greater confidence as a false positive. These candidates are ignored for this report.

It is important to stress that this ranking system is subjective. In practice for this project, one interpreter performed two iterations over the entire imagery database in order to increase the internal consistency of the approach. This task took approximately two full weeks. A second interpreter independently ranked each candidate identified by the first interpreter. Then, a third interpreter blindly ranked the candidates for which the two previous interpreters disagreed. The lowest confidence rank (i.e. highest slick potential) was kept as the candidate's final confidence level in the GIS database. Finally, wind speed data and chlorophyll-*a* data (see Section 3.2) were used to help screen out probable look-alikes from candidates with a confidence rank of 1 or 2.

3.2 Semi-automated analysis

An automated detection algorithm for dark spots was also developed and implemented. Its main goals were to help interpreters focalize on areas of potential seeps to avoid inspection of the entire set of imagery and to provide a less subjective set of oil slick candidates than the visual interpretation method. Our approach is based on image segmentation followed by region thresholding (see Topouzelis 2008 for a review of prevalent approaches). The main steps of the automated component of the method are shown in Figure 2.

The SAR data pre-processing includes geocoding, calibration and image filtering (3 × 3 median filter), followed by a normalization of the backscatter along the range direction based on the CMOD5 model (Hersbach et al., 2007) with a wind speed of 3 m/s and wind direction relative to north of 90 degrees. Then, the contrasted limited adaptive histogram enhancement (CLAHE) algorithm (Zuiderveld, 1994) is applied to reduce large scale background variability and to enhance local contrast. CLAHE tiles size are set to 400 pixels on a side. Next, the CLAHE image is partitioned into homogeneous regions with the Simple Linear Iterative Clustering (SLIC) algorithm (Achanta et al., 2012) with a grid size of 256 pixels. This is followed by a hierarchical region growing algorithm to merge spatially connected regions so that all region sizes must be larger than a specific size (~16×10^3 ha). The latter size was determined empirically from visual inspection of images. To detect dark pixels, a threshold is applied on each region of the region grown CLAHE image. The threshold is given in unit of median of absolute deviation below the region median. The backscatter characteristics within and surrounding each dark spot are computed (e.g. intensity mean, standard deviation, area, etc.). Moreover, auxiliary data such as wind speed data (National Synthetic Aperture Radar (SAR) Winds (NSW) Products, Environment and Climate Change Canada) and chlorophyll-*a* data derived from MODIS[1] are also extracted around each dark spot, if available. Regional information such as the density (number) of dark spots in a same region, distance from high wind areas, and distance from coast were also considered (Konik and Bradtke, 2016). These features are ingested by a fuzzy logic engine to generate a plausibility score, S, $0 \leq S \leq 1$, for each dark spot. The fuzzy membership functions for favorable wind speed regime and intensity contrast between the dark spot and its surrounding were defined with values taken from the literature; basically the following criteria have been used: winds between 3 and 8 m/s, contrast greater than 3 dB and chlorophyll-*a* concentration smaller than 0.2 mg/m^3. The other membership functions were determined empirically. The computer processing time of the current implementation is about 30 minutes per image.

The outline of each dark spot was vectorized and saved with their associated attributes in a shapefile for each Radarsat-2 image. A threshold, T_S, was applied on the dark spot scores to eliminate *i*) the more obvious look-alikes and *ii*) false positives obtained at the thresholding step of the region grown CLAHE image. The threshold was determined with the help of ranks 1 and 2 candidates found by the visual method of Section 3.1. The low-scores dark spots basically represent cases where intensity contrast is too low, winds are too low or too high, or where chlorophyll-*a* is detected.

[1] https://oceandata.sci.gsfc.nasa.gov/MODIS-Aqua/Mapped/Monthly/4km/chlor_a

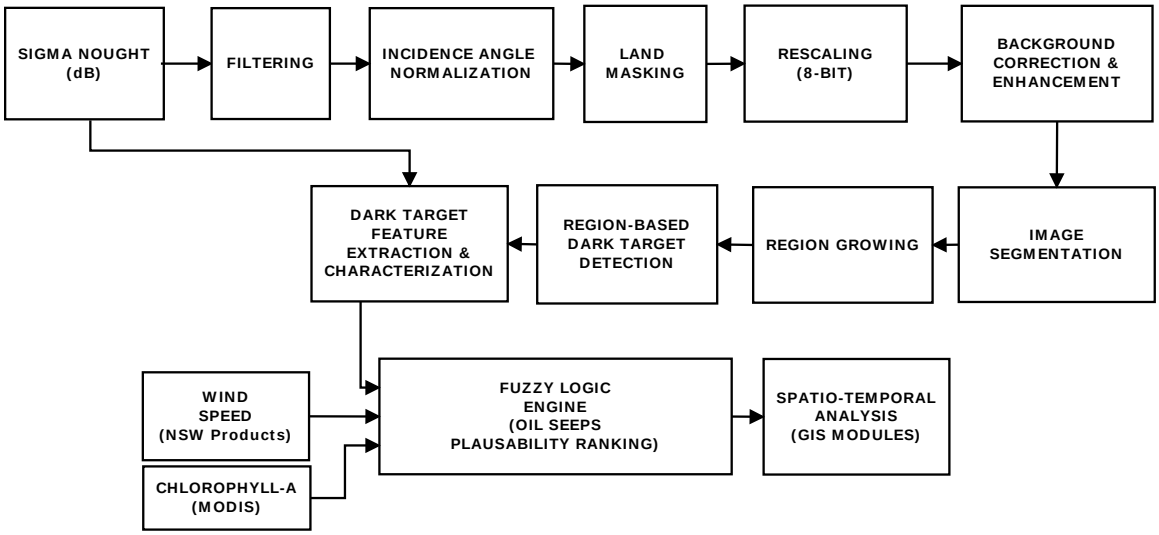

Figure 2. Dark spot processing chain.

The second component of the semi-automated method (not included in Figure 2) relies on visual interpretation (non-automated part of the method). In a first step, all dark spots above T_s are visually inspected to eliminate unambiguous look-alikes and false positives. In the present case, this corresponded to 2700 dark spots, or on average, one dark spot per 10650 km^2 (~2 per Radarsat-2 scene). A graphical interface was developed within Matlab to quickly visualize and assign look-alike status by simple mouse clicking. This generated a file of dark spots ready to be ingested into a GIS. Although it can only take a few seconds to inspect each spot, as their look-alike status must be unambiguous, this step took two days nevertheless to visually assess 2700 dark spots. In the final step, the interpreter ranked the remaining dark spots above $T_{s,}$ not assigned a look-alike status, according to the same ranking system as described in 3.1. The ranking (confidence level) is added in a GIS database.

3.3 GIS integration, analysis and visualization

A dedicated GIS toolbox was developed to ingest and analyse the vectorized seep candidates and their associated attributes. Figure 3 shows the main modules of the processing chain for images from years 2015, 2016, and 2017. The toolbox is designed to assess and visualize the spatio-temporal distribution of the dark spots (potential oil slicks). The first module builds a database for each year from the dark spot shapefiles obtained by either the visual interpretation (section 3.1) or the semi-automated approach (section 3.2). These databases are aimed at investigating the spatio-temporal distribution within a single year (August to October). Next, a master geodatabase is constructed to conduct inter-year spatio-temporal analysis. Note that Chlorophyll-*a* concentration within each image footprint are automatically retrieved from MODIS Aqua Level 3 Global Monthly Mapped 4 km Chlorophyll-*a* product[1] (Hu et al. 2012).

The second module computes spatio-temporal groupings based on neighbouring analysis of seep candidates. A search for adjacent seep candidates is performed in the vicinity of the seep candidates within a predefined radius to identify possible clusters in the spatial domain, then in the time dimension. The goal of this module is to search for temporal coincidence of seep candidates in a same area, both within a year and between-years, to assess the seep origin likelihood of the dark spots, in any.

The third module is a designed interface to facilitate both global and local visualisation of seep candidates and their possible clustering. This module generates a '.mxd' file for interactive visual analysis of seep candidates. For example, one tool developed for the module retrieves, through simple mouse actions, the Radarsat-2 image from which the seep candidate was identified. This allows the user, if necessary, to revise the confidence level status of any seep candidate in the database. A density map (heat maps) is also displayed to demonstrate the spatial variability of seep candidates. Clusters, if present, are labelled according to an encoding schema that indicates the number of months between the acquisition date for the seep candidates; the number of seep candidates contained in a group is recorded as a shared attribute.

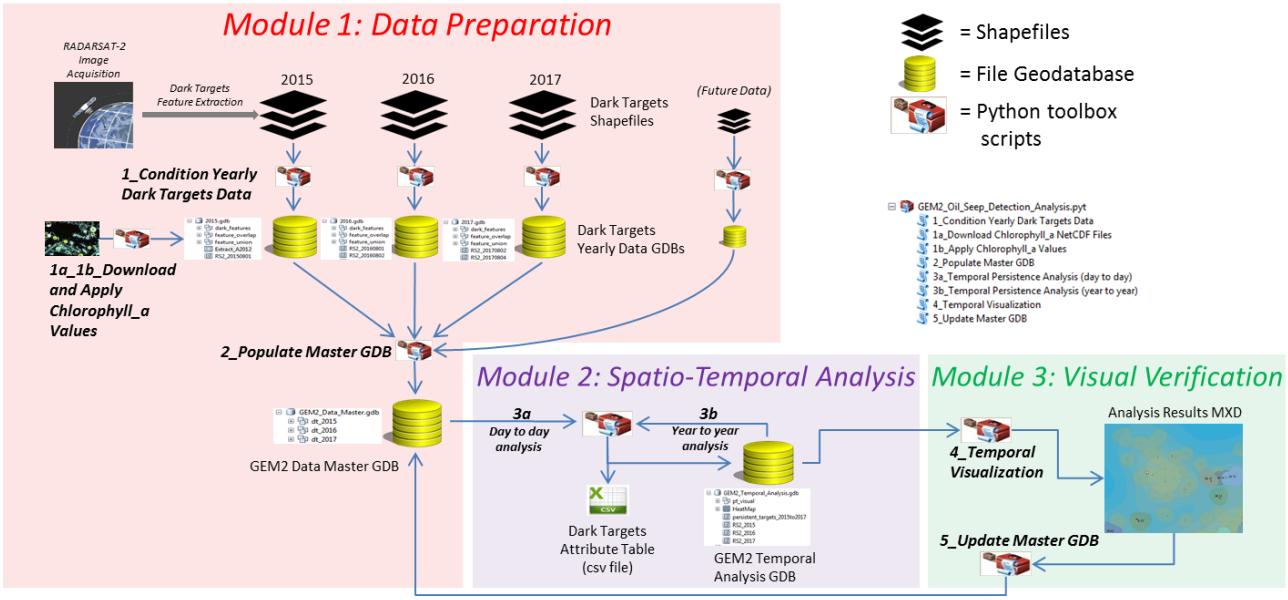

Figure 3. GIS modules for data integration, analysis and visualization.

4. RESULTS

The list of dark spots retained as oil slick candidates is given in Table 1. The list contains 33 geographic locations of candidates with confidence ranks of 1 or 2. The corresponding Radarsat-

2 image subsets for each oil slick candidate are shown in Figure 4. Notice that no distinction is made in Table 1 between ranks 1 and 2 candidates as they can all be considered as belonging to rank 2. The Annex presents the same dark spots subset with higher contextual views.

In total, the visual interpretation method identified 25 oil slick candidates and the semi-automated method identified 22 oil slick candidates. A comparison of the two approaches (Sections 3.1, 3.2) reveals that 11 out of the 33 candidates are uniquely selected by the visual method whereas 5 candidates were detected uniquely by the semi-automated method. Thus, only 14 candidates are shared between the two approaches. Moreover, two dark spots were identified during the look-alike rejection step of the semi-automated method on other image parts (marked by the letter 'M' in their Id labels). Candidate Id's in Table 1 containing the letter 'A' refers to dark spots uniquely identified by the automated method.

One of the major expectation of this project was to look for persistence over time of seep candidates concentrated over a same region in order to assist in finding regions with a greater likelihood of oil seep origin. Unfortunately, the results do not convincingly support the oil seep origin of any dark spot. Figure 5 shows the distribution and spatio-temporal grouping of the candidates listed in Table 1, which has been augmented with the candidates of ranks 1 and 2 given in the GSC open file 7070 (Decker et al. 2013b). Solely for internal consistency considerations along the 2010-2012 2015-2017 time sequence, candidates in the latter list where either chlorophyll-*a* presence (phytoplankton) or too high/low wind conditions are suspected were not considered in the analysis (Table 2).

Group labels in Table 1, fifth column, and Figure 5 are coded so that the first digit provides a group identification number and the second two digits gives the number of months between image acquisitions (the group identification number is arbitrary and has no meaning). There are two co-occurrences, identified as '7.12' and '8.11' in Table 1 and Figure 5, in the 2015-2017 survey. Each occurrence is about one year apart with one pair separated by 23 km with the other separated by 38 km. The third co-occurrence, referred to group '2.72' in Table 1 and Figure 5, involved candidates from the 2010-2012 survey, specifically FOX_2010_003 and FOX_2010_004 which are in the vicinity of HS_2016_09. The pairwise distance is 20 km. Group '1.1' consists of two occurrences 34 days (year 2015) apart and separated by 35km.

Table 1. Dark spot locations (highest confidence ranking for potential slicks).

Dark spot Id	Radarsat-2 Id	Longitude (degrees)	Latitude (degrees)	Group Id*	Minimum Pairwise Distance (km)
HS_2015_47	RS2_OK67336_PK615405_DK546511_W2_20150918_224349_VV_SGF	-79.79027655	64.81975687		
HS_2015_50***	RS2_OK67337_PK615455_DK546561_W2_20150925_224029_VV_SGF	-80.02594876	68.63325302	7.12	23
HS_2015_51	RS2_OK67337_PK615461_DK546567_W2_20150926_234942_VV_SGF	-94.50982345	59.98513308		
HS_2015_57	RS2_OK67337_PK615460_DK546566_W2_20150926_234921_VV_SGF	-92.73846392	59.99711935		
HS_2015_58***	RS2_OK67337_PK615468_DK546574_W2_20150927_232106_VV_SGF	-88.06217817	62.95003896		
HS_2015_61	RS2_OK68499_PK624186_DK554947_W2_20151002_223453_VV_SGF	-74.71374081	63.59616599		
HS_2015_76***	RS2_OK68500_PK624287_DK554898_W2_20151021_232047_VV_SGF	-86.99314669	62.14867588		
HS_2015_77***	RS2_OK68500_PK624291_DK554902_W2_20151022_225052_VV_SGF	-78.98060594	60.31248521		
HS_2015_A1	RS2_OK67337_PK615478_DK546584_W2_20150928_225245_VV_SGF	-81.15396846	67.60585111		
HS_2015_A2	RS2_OK68499_PK624233_DK554994_W2_20151011_231203_VV_SGF	-84.42934917	61.74952669	1.1	35
HS_2015_A4	RS2_OK68500_PK624268_DK554879_W2_20151017_233717_VV_SGF	-89.74938576	61.52454507		
HS_2015_M1	RS2_OK67335_PK615523_DK546444_W2_20150907_230359_VV_SGF	-83.74563205	61.79708124	1.1	35
HS_2016_09**	RS2_OK80494_PK709818_DK637558_W2_20161013_223909_VV_SGF	-78.75114525	64.34430896	2.72	20
HS_2016_10	RS2_OK80495_PK709845_DK637585_W2_20161021_220440_VV_SGF	-68.14406681	61.61077289		
HS_2016_101	RS2_OK80495_PK709828_DK637568_W2_20161015_232031_VV_SGF	-85.64588111	62.22049698		
HS_2016_102	RS2_OK80495_PK709827_DK637567_W2_20161015_232010_VV_SGF	-86.11366802	61.72863207		
HS_2016_108	RS2_OK80495_PK709863_DK637603_W2_20161025_232838_VV_SGF	-87.48744325	61.30889959		
HS_2016_37***	RS2_OK78288_PK692675_DK621935_W2_20160820_235337_VV_SGF	-93.04233142	60.57673045		
HS_2016_45***	RS2_OK79254_PK699589_DK628399_W2_20160903_234431_VV_SGF	-92.55185737	58.52148856		
HS_2016_47***	RS2_OK79254_PK699607_DK628417_W2_20160907_232716_VV_SGF	-85.40526571	56.21721238		
HS_2016_48***	RS2_OK79254_PK699618_DK628428_W2_20160910_234015_VV_SGF	-90.82449564	57.64633076		
HS_2016_78***	RS2_OK79261_PK699763_DK628552_W2_20160929_224836_VV_SGF	-79.97506258	68.43022438	7.12	23
HS_2016_79	RS2_OK79261_PK699763_DK628552_W2_20160929_224836_VV_SGF	-81.45122231	68.42149528		
HS_2016_90	RS2_OK80494_PK709794_DK637534_W2_20161009_225421_VV_SGF	-79.21749734	58.52738789	8.11	38
HS_2016_95	RS2_OK80494_PK709811_DK637551_W2_20161012_230652_VV_SGF	-82.00525965	59.12991529		
HS_2016_A5	RS2_OK79261_PK699691_DK628480_W2_20160919_223850_VV_SGF	-77.64145773	62.74816018		
HS_2017_00***	RS2_OK87868_PK780120_DK708992_W2_20170816_232448_VV_SGF	-87.87418704	64.30029472		
HS_2017_21	RS2_OK90435_PK800939_DK728828_W2_20170916_231847_VV_SGF	-84.77279658	57.23737481		
HS_2017_25	RS2_OK90435_PK800969_DK728858_W2_20170920_230219_VV_SGF	-80.00932474	58.57815316	8.11	38
HS_2017_43	RS2_OK91353_PK808423_DK736264_W2_20171005_222726_VV_SGF	-76.825837	68.273362		
HS_2017_46	RS2_OK91353_PK808428_DK736269_W2_20171006_233640_VV_SGF	-91.17768786	61.24814493		
HS_2017_A6	RS2_OK91355_PK808521_DK736426_W2_20171016_234511_VV_SGF	-91.79409702	61.59313693		
HS_2017_M1	RS2_OK91355_PK808561_DK736466_W2_20171028_225359_VV_SGF	-78.80606816	58.88465578		

* First number provides the group identification number, the second two digits the number of months between images (see Figure 5).

** The other dark spots in the vicinity of HS_2016_09 are FOX_2010_0003 and FOX_2010_004 (GSC Open File 7070).

*** Dark spots uniquely identified by the visual approaches.

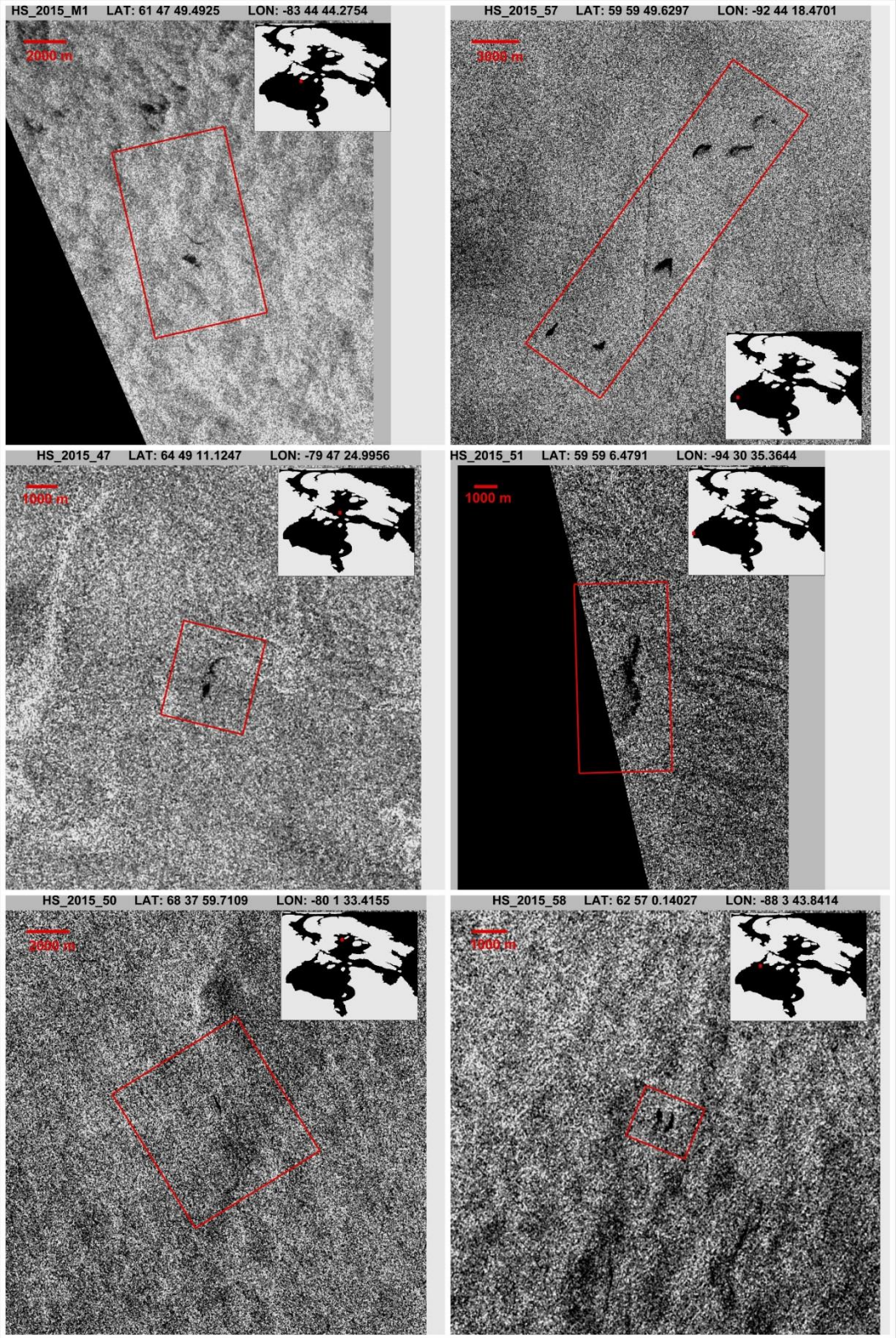

Figure 4. Dark spots categorized as best potential oil slicks. Inset shows geographic location on the map. North on top.

Figure 4. (continued)

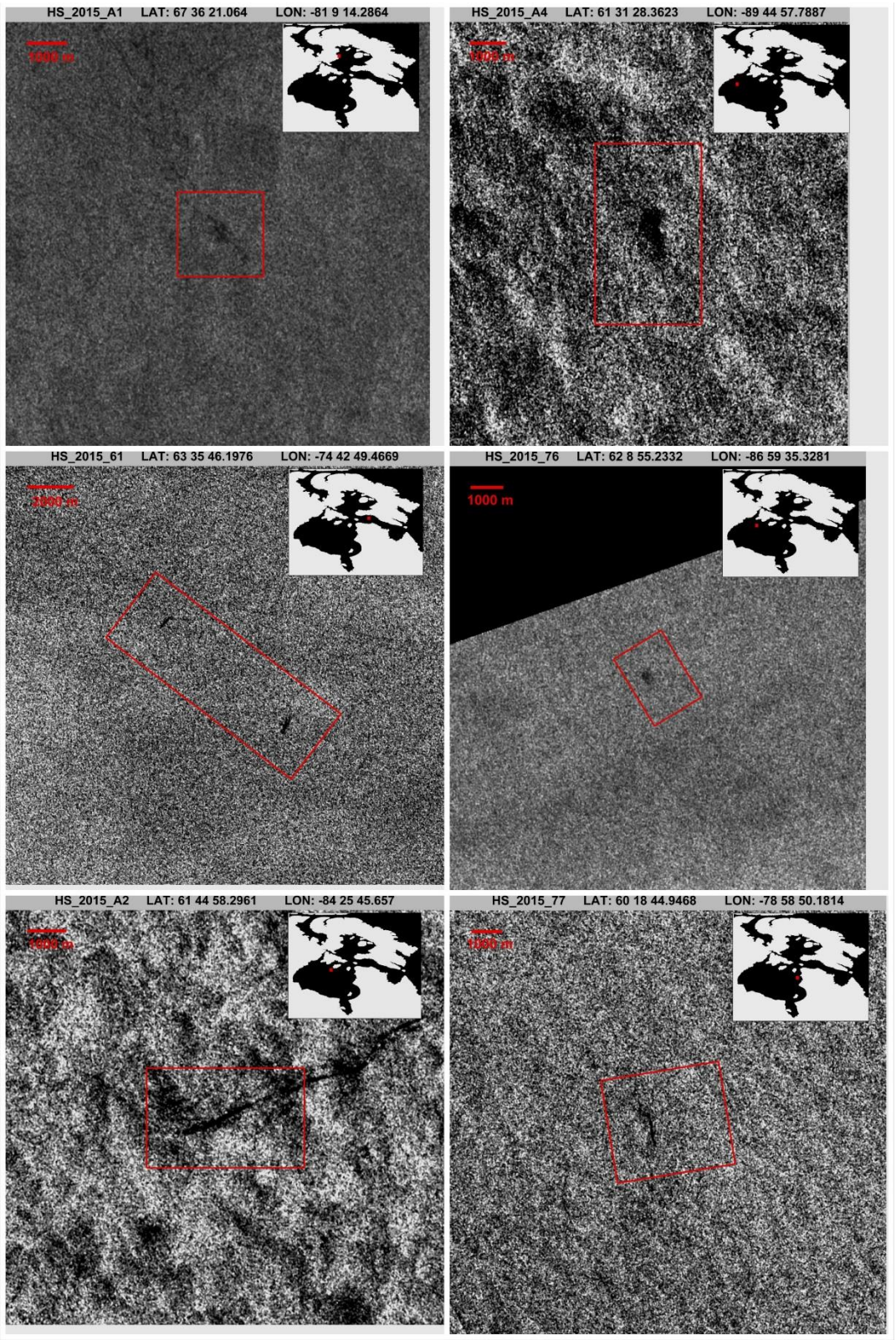

Figure 4. (continued)

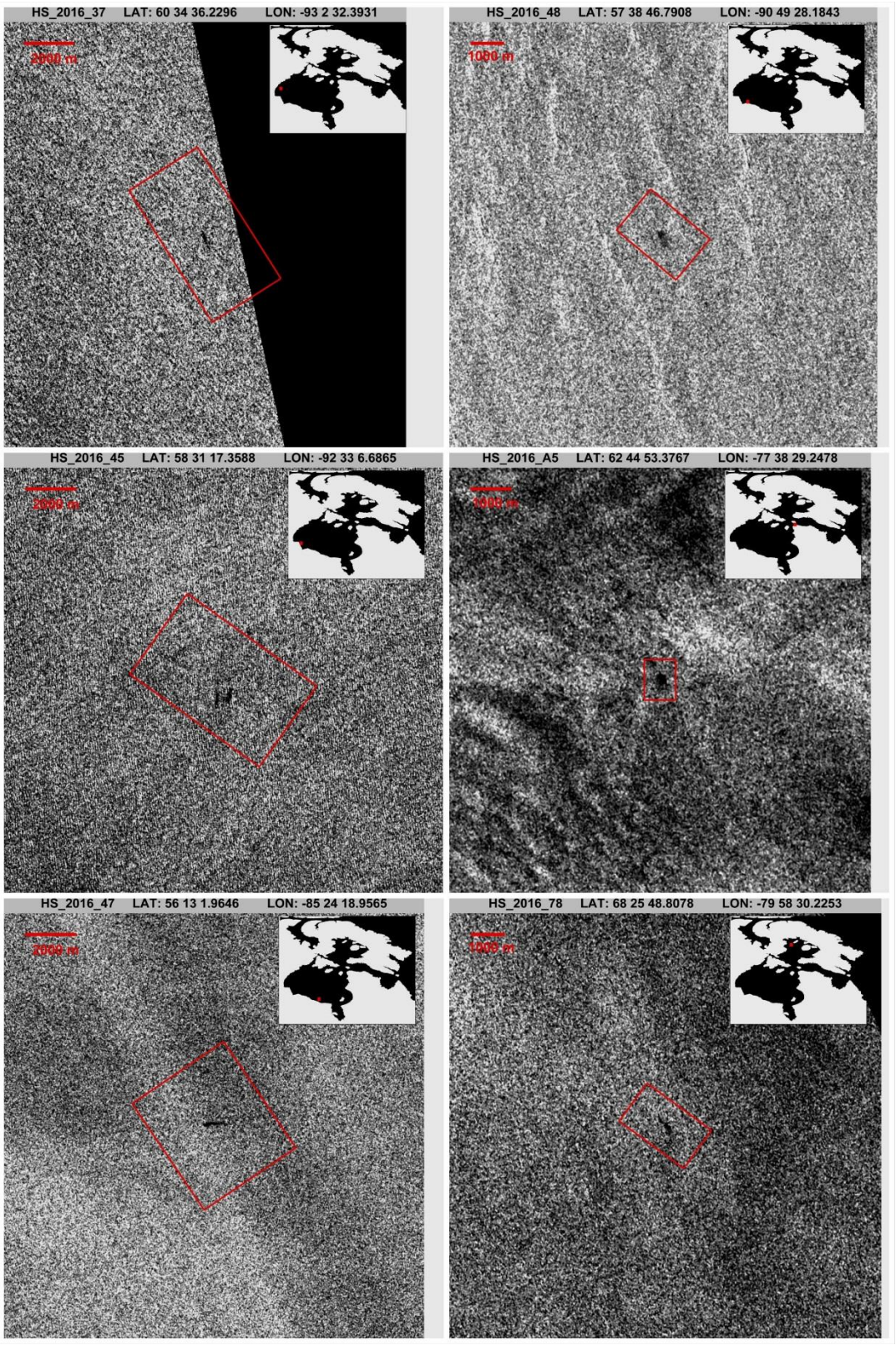

Figure 4. (continued)

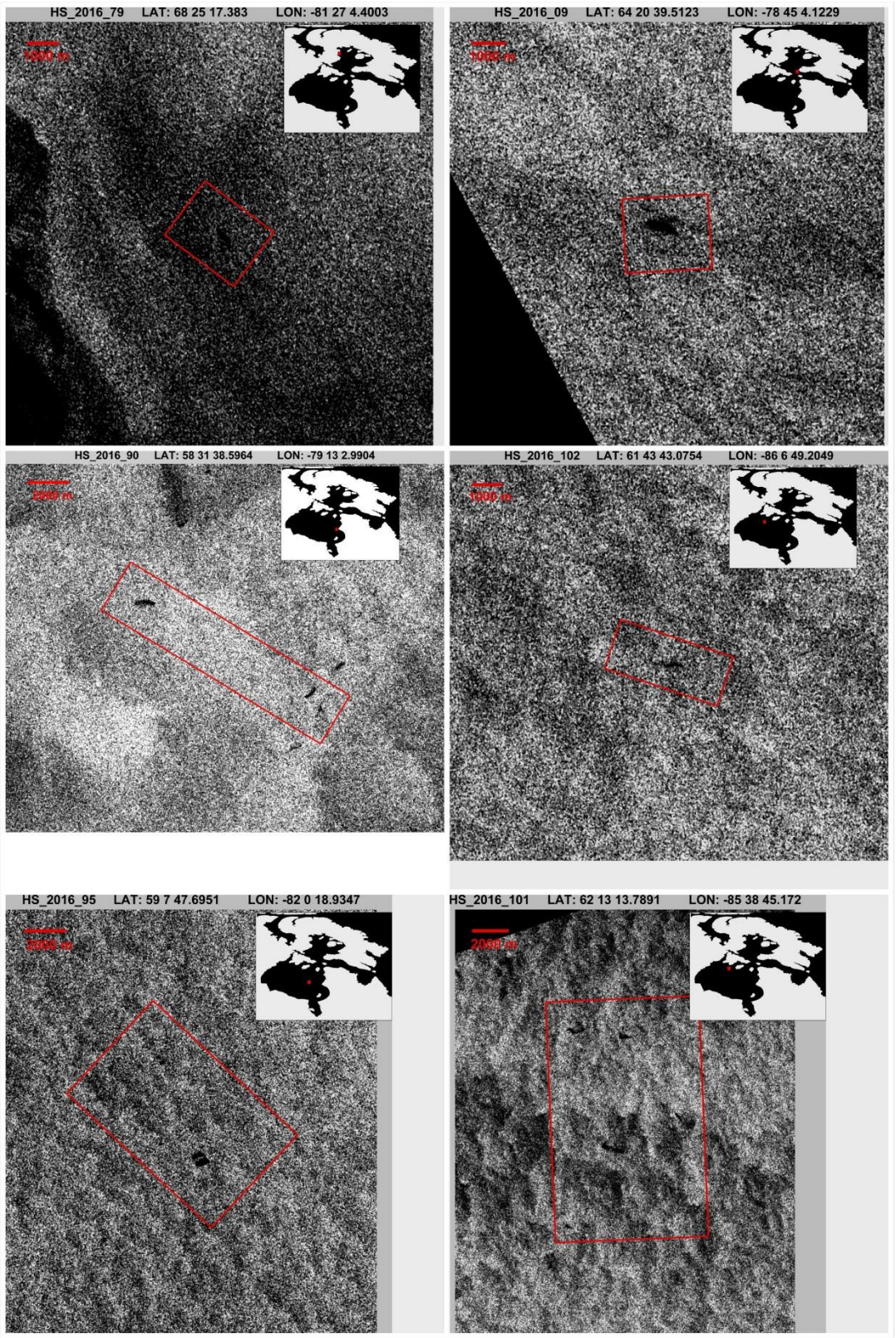

Figure 4. (continued)

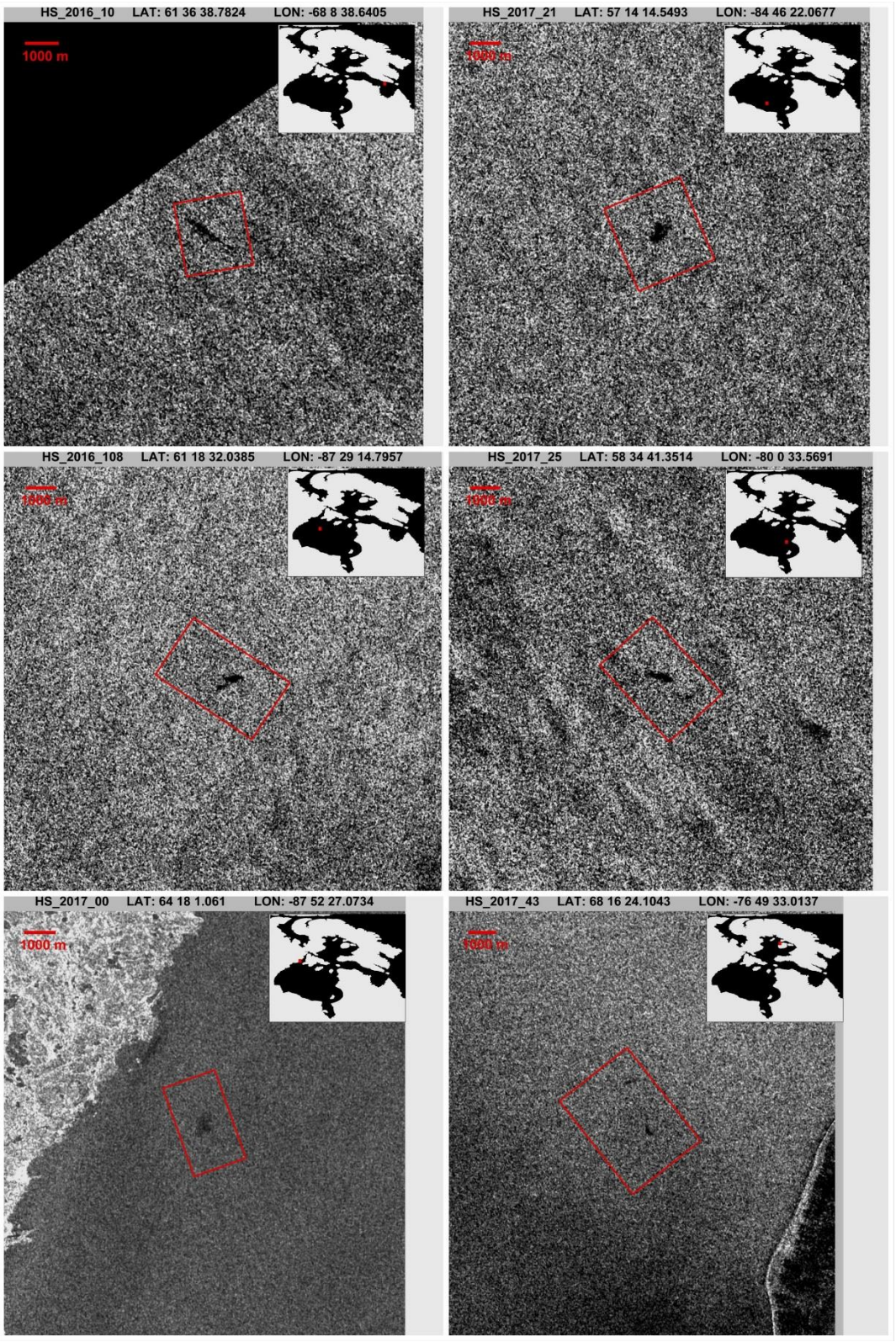

Figure 4. (continued)

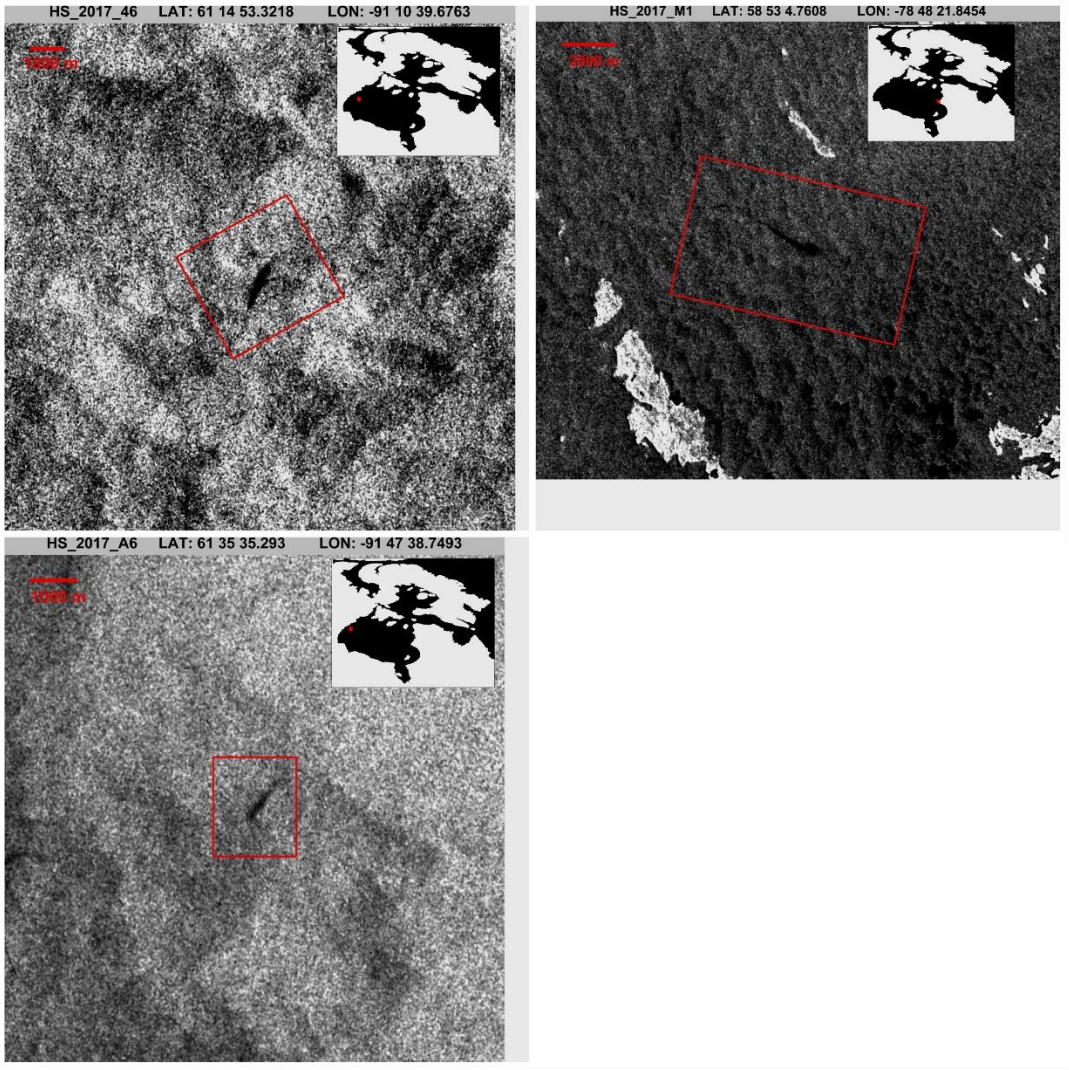

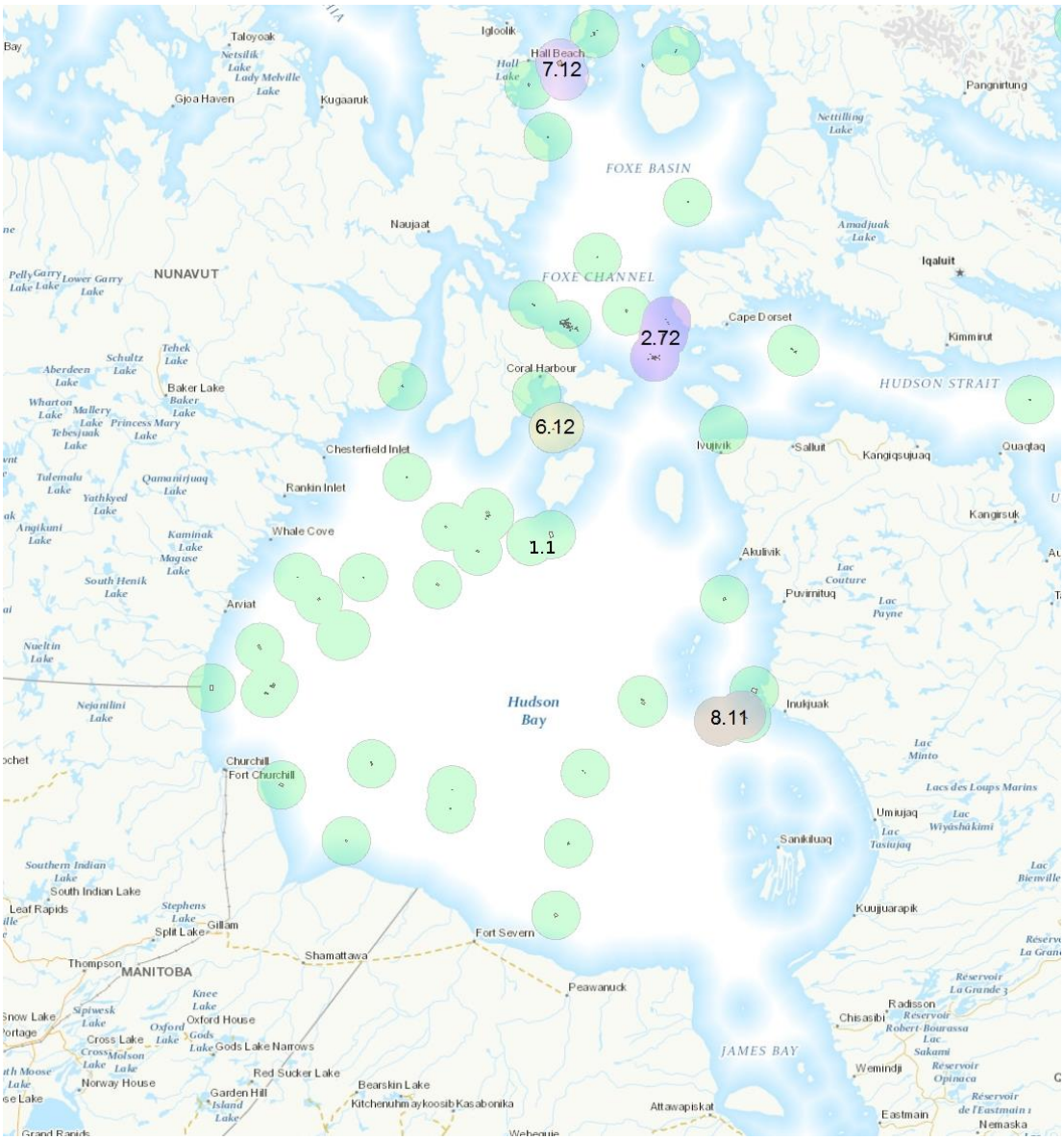

Figure 5. Location of oil slick candidates. Disks with numbers indicates potential slick spatio-temporal co-occurrences. See Section 4 and Table 1 for details. Pair 6.12 was identified in Decker et al. (2013b).

Table 2. Dark spots with ranking < 3 that are located in an area where the presence of chlorophyll-*a* or low/high wind speeds conditions is suspected.

Dark Target Id (GSC OF7070)	Chlorophyll-*a* (mg/m^3)	Number of days from Radasat-2 acquisition	Wind Speed (m/s)
Fox-2012_001	0.56	-1	
Hud-2010_004	0.73	2	
Hud-2010_009	1.97	-2	
Hud-2011_002	4.40	0	
Hud-2012_002	1.10	0	
Hud-2012_008	0.69	0	
Hud-2012_010	0.63	0	
Hud-2012_011	0.36	-1	
Hud-2012_014	1.27	1	
FOX_2011_002			14
FOX_2012_004			12
HUD_2010_001			9
HUD_2010_002			9
HUD_2012_007			2

5. CONCLUSIONS

This work reports the results from the analysis 1278 Radasat-2 images for oil slicks detection. The final list contains 33 oil slick candidates. The number of candidates selected uniquely from visual inspection of the entire imagery account for 25 candidates. The number of candidates obtained from the semi-automated approach equals 22 candidates. The number of candidates shared between the two approaches is 14. There is thus complementarity between the two approaches. However, if such a work would be repeated, it would be much easier for an interpreter to learn to recognize the type of dark spots detected with the semi-automated but missed by the visual approach, than to tuning or re-designing the automated algorithm to catch the 11 missed candidates. The usefulness of wind speed and chlorophyll-*a* data to help remove suspected look-alikes is unequivocal and had a significant impact on our oil slick ranking system.

Considering the short time frame and the relatively low number of observation per square kilometre, the spatio-temporal analysis does not significantly reinforce the presence of a natural origin of any detected dark spots. Definite persistence of dark spots in a same area was not observed, with only a few observed pairs of candidates separated by a large distance. Nevertheless, the information gathered in this report may help future works focus on the few areas that show more dense occurrences of slick candidates.

Observations that are more frequent and a longer time series would be beneficial to this approach. In this regard, the Radarsat constellation Mission and other systematic sensors such as Sentinel-1 would prove valuable tool for further research. Moreover, the availability of the complete Sentinel-1 archive in data cubes such as the Google earth-engine represent another opportunity for further research.

In future works, because our GIS module can easily and quickly retrieve chlorophyll-*a* data, we would suggest to proceed by the visual interpretation approach using the chlorophyll-*a* information to reject look-alikes at the early interpretation stage (e.g. masking/marking sea areas with high chlorophyll-*a* concentration). Then, only for the selected seep candidates, retrieve the wind speed data for further discrimination of look-alikes.

ACKNOWLEDGMENTS

The authors are grateful to Dr. François Charbonneau for reviewing this report and providing constructive comments.

REFERENCES

Achanta, R., Shaji, A., Smith, K., Lucchi, A., Fua, P., and Süsstrunk, S., 2012. SLIC Superpixels Compared to State-of-the-art Superpixel Methods, IEEE Trans. Pattern Analysis and Machine Intelligence 34, 2274 – 2282.

Alpers, W., Holt, B., Zeng, K., 2017. Oil spill detection by radar imaging radar: challenges and pitfalls, Remote Sensing of Environment 201, 133-147.

Decker, V., Budkewitsch, P., Tang, W., 2013a. Database of suspect oil seeps in the marine environment of Baffin Bay and Davis Strait, Nunavut, identified from a survey of RADARSAT-2 data; Geological Survey of Canada, Open File 7404.

Decker, V., Budkewitsch, P., and Tang, W., 2013b. Reconnaissance Mapping of Suspect Oil Seep Occurrences in Hudson Bay and Foxe Basin Using Satellite Radar; Geological Survey of Canada, Open File 7070.

Hersbach, H., Stoffelen, A., de Haan, S., 2007. An improved C-band scatterometer ocean geophysical model function: CMOD5. Journal of Geophysical Research, 112, C03006.

Hu, C., Lee, Z. and Franz, B. A., 2012. Chlorophyll-a algorithms for oligotrophic oceans: A novel approach based on three-band reflectance difference, J. Geophys. Res., 117, C01011, doi:10.1029/2011JC007395.

Konik, M. and Bradtke, K., 2016. Object-oriented approach to oil spill detection using ENVISAT ASAR images, ISPRS Journal of Photogrammetry and Remote Sensing 118, 37-52.

Topouzelis, K. N., 2008. Oil Spill Detection by SAR Images: Dark Formation Detection, Feature Extraction and Classification Algorithms, Sensors 8, 10, 6642-6659.

Zuiderveld, K., Contrast limited adaptive histogram equalization. Graphic gems IV. San Diego: Academic Press Professional, 1994. p. 474-485.

ANNEX. Larger extent views of oil slick candidates.

The following figures provides larger extent views around each dark spots (same order as in Figure 4).

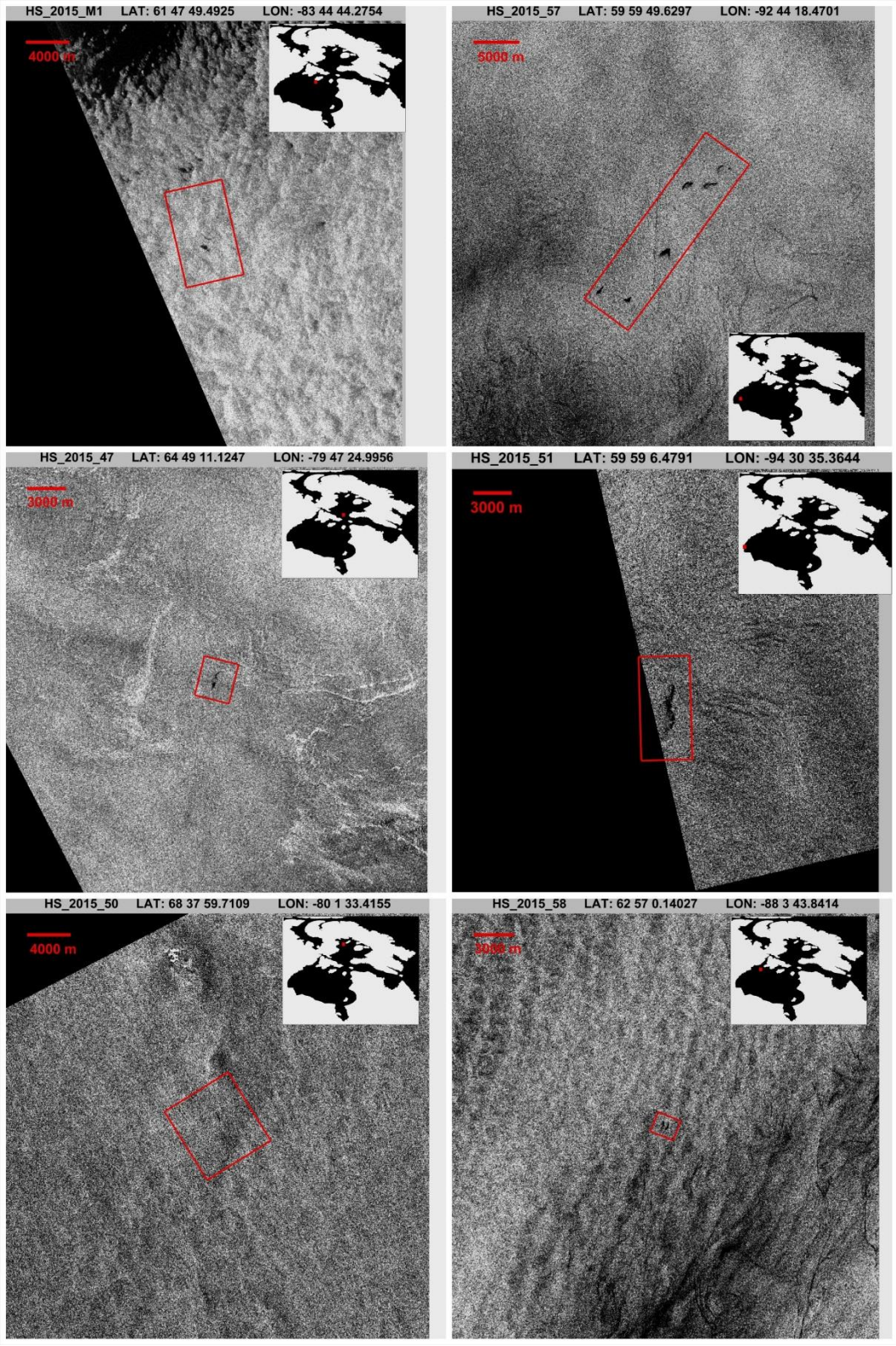

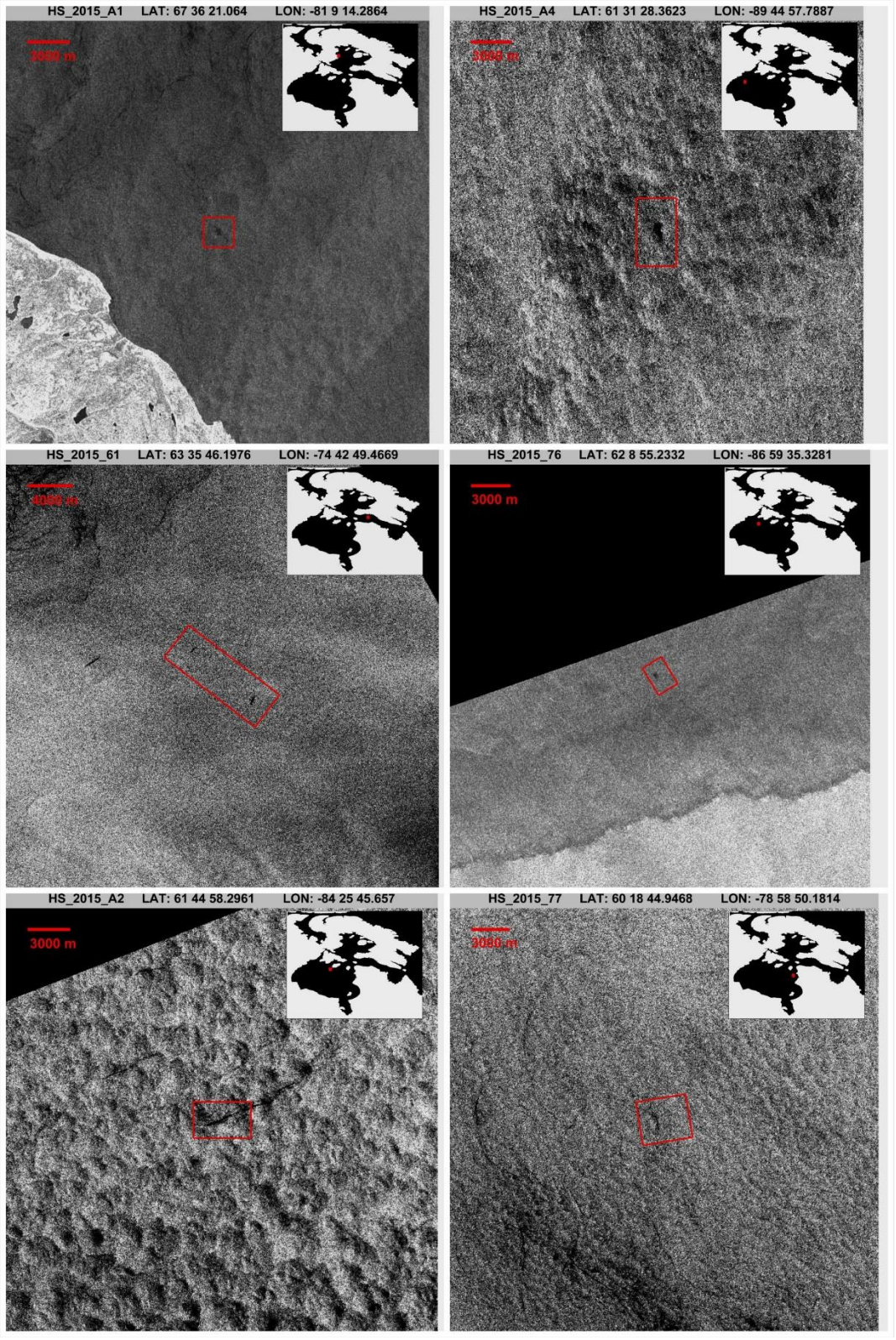
HS_2015_A1 LAT: 67 36 21.064 LON: -81 9 14.2864
3000 m
HS_2015_A4 LAT: 61 31 28.3623 LON: -89 44 57.7887
3000 m
HS_2015_61 LAT: 63 35 46.1976 LON: -74 42 49.4669
3000 m
HS_2015_76 LAT: 62 8 55.2332 LON: -86 59 35.3281
3000 m
HS_2015_A2 LAT: 61 44 58.2961 LON: -84 25 45.657
3000 m
HS_2015_77 LAT: 60 18 44.9468 LON: -78 58 50.1814
3000 m

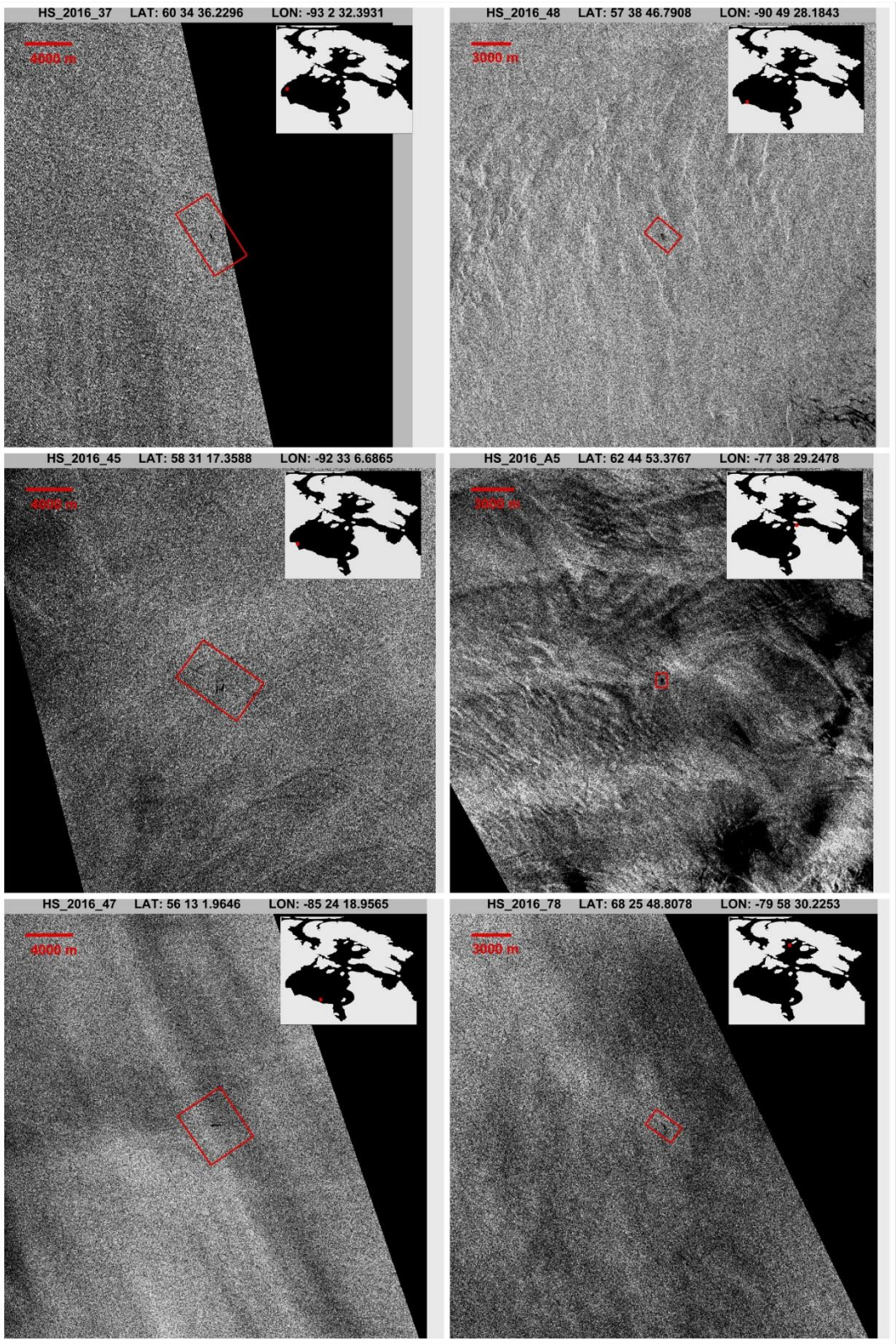
HS_2016_37 LAT: 60 34 36.2296 LON: -93 2 32.3931
3000 m
HS_2016_48 LAT: 57 38 46.7908 LON: -90 49 28.1843
3000 m
HS_2016_45 LAT: 58 31 17.3588 LON: -92 33 6.6865
3000 m
HS_2016_A5 LAT: 62 44 53.3767 LON: -77 38 29.2478
3000 m
HS_2016_47 LAT: 56 13 1.9646 LON: -85 24 18.9565
3000 m
HS_2016_78 LAT: 68 25 48.8078 LON: -79 58 30.2253
3000 m

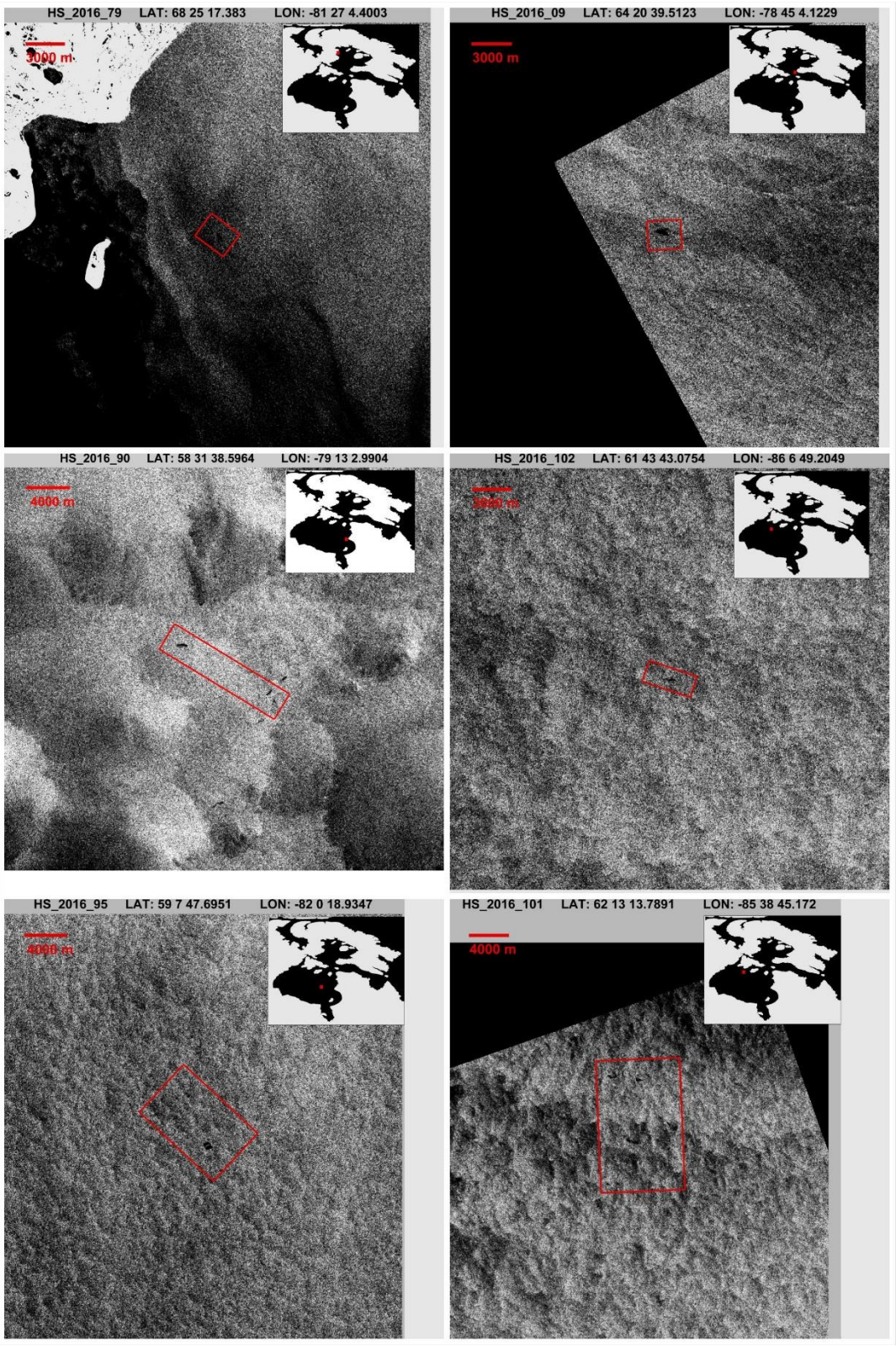
HS_2016_79 LAT: 68 25 17.383 LON: -81 27 4.4003
3000 m
HS_2016_09 LAT: 64 20 39.5123 LON: -78 45 4.1229
3000 m
HS_2016_90 LAT: 58 31 38.5964 LON: -79 13 2.9904
4000 m
HS_2016_102 LAT: 61 43 43.0754 LON: -86 6 49.2049
HS_2016_95 LAT: 59 7 47.6951 LON: -82 0 18.9347
HS_2016_101 LAT: 62 13 13.7891 LON: -85 38 45.172
4000 m

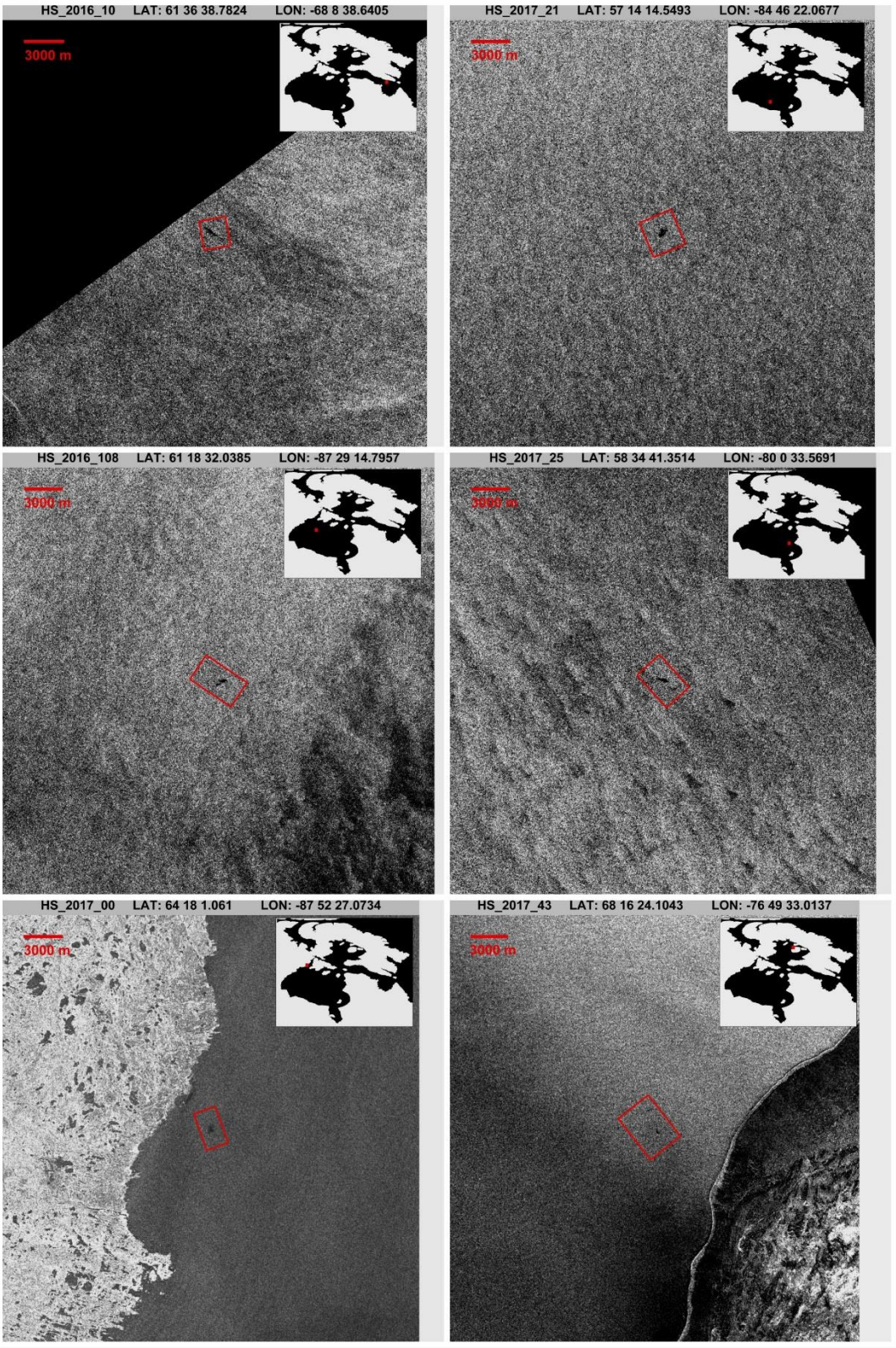
HS_2016_10 LAT: 61 36 38.7824 LON: -68 8 38.6405
3000 m
HS_2017_21 LAT: 57 14 14.5493 LON: -84 46 22.0677
3000 m
HS_2016_108 LAT: 61 18 32.0385 LON: -87 29 14.7957
3000 m
HS_2017_25 LAT: 58 34 41.3514 LON: -80 0 33.5691
3000 m
HS_2017_00 LAT: 64 18 1.061 LON: -87 52 27.0734
3000 m
HS_2017_43 LAT: 68 16 24.1043 LON: -76 49 33.0137
3000 m

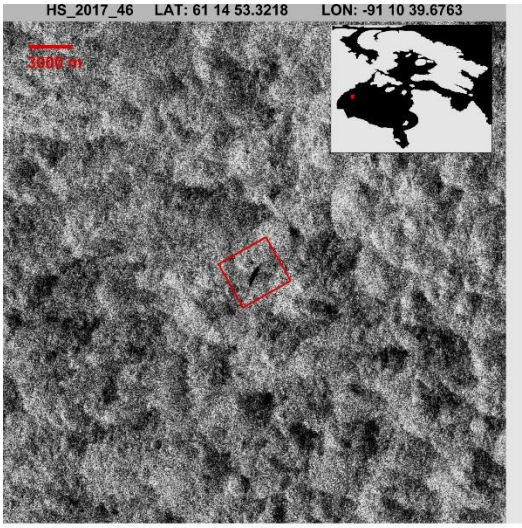
HS_2017_46 LAT: 61 14 53.3218 LON: -91 10 39.6763
3000 m

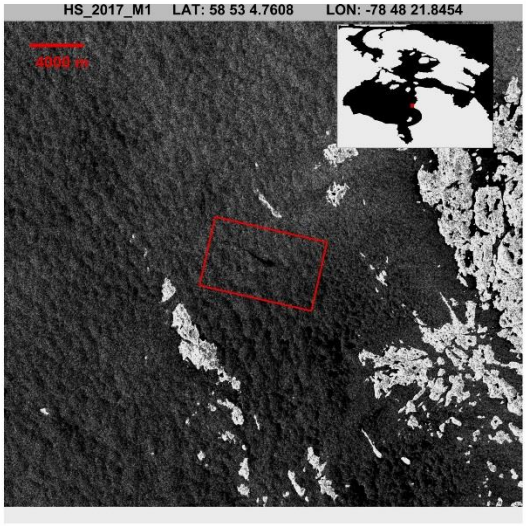
HS_2017_M1 LAT: 58 53 4.7608 LON: -78 48 21.8454
4000 m

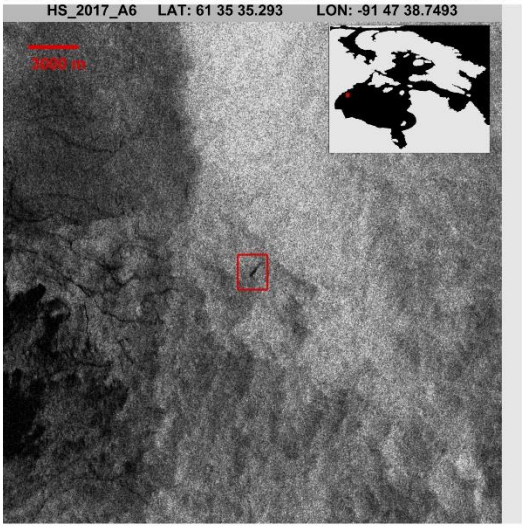
HS_2017_A6 LAT: 61 35 35.293 LON: -91 47 38.7493
3000 m